Published in final edited form as:

*Clin Imaging*. 2016 ; 40(5): 1047–1054. doi:10.1016/j.clinimag.2016.06.002.

# Diffusion weighted imaging reflects variable cellularity and stromal density present in breast fibroadenomas

**Sana Parsian, MD**,

PGY4 radiology resident, University of Washington School of Medicine, Department of Radiology, Seattle Cancer Care Alliance, 825 Eastlake Ave. E., G3-200, Seattle, WA 98109-1023, Phone: (206) 288-1306, Fax: (206) 288-6473, Disclosure: None

**Nadia V. Giannakopoulos, MD, PhD**,

Affiliation at the time of the study: Department of Anatomic Pathology, University of Washington School of Medicine, 1959 NE Pacific St., Box 356100, Seattle, WA 98195, Phone: 206-598-1393, Fax: 206-598-3803, Disclosure: None, Present affiliation and address: Assistant Professor of Pathology, University of Alberta, Department of Laboratory Medicine and Pathology, 5B4.57 WMC, 8440 112 ST NW, Edmonton, Alberta, Canada T6G 2B7, Phone: 780-407-1668, Fax: 780-407-3009, Disclosure: None

**Habib Rahbar, MD**,

Assistant Professor of Radiology, University of Washington School of Medicine, Department of Radiology, Seattle Cancer Care Alliance, 825 Eastlake Ave. E., G3-200, Seattle, WA 98109-1023, Phone: 206-288-1257, Fax: (206) 288-6473, Disclosure: None

**Mara H. Rendi, MD, PhD**,

Assistant Professor of Pathology, Department of Anatomic Pathology, University of Washington School of Medicine, 1959 NE Pacific St., Box 356100, Seattle, WA 98195, Phone: 206-598-1393, Fax: 206-598-3803, Disclosure: None

**Xiaoyu Chai, MS**, and

Statistical Research Associate, Department of Biostatistics & Biomathematics, Fred Hutchinson Cancer Research Center, 1100 Fairview Ave N, M2-B500, Seattle, WA 98109, Phone: 206-667-3004, Disclosure: None

**Savannah Partridge, PhD**

Research Professor of Radiology, University of Washington School of Medicine, Seattle Cancer Care Alliance, 825 Eastlake Ave. E., G3-200, Seattle, WA 98109-1023, Phone: (206) 288-1306, Fax: (206) 288-6473, Disclosure: None

Sana Parsian: parsian@uw.edu; Nadia V. Giannakopoulos: ngiannak@ualberta.ca; Habib Rahbar: hrahbar@uw.edu; Mara H. Rendi: mararend@uw.edu; Xiaoyu Chai: xchai@fredhutch.org; Savannah Partridge: scp3@u.washington.edu

Correspondence to: Savannah Partridge, `scp3@u.washington.edu`.

This HIPAA-compliant retrospective study had institutional review board approval, and the need for informed patient consent was waived.

## Abstract

**OBJECTIVE—**To determine the underlying histopathologic features influencing apparent diffusion coefficient (ADC) values of breast fibroadenomas.

**MATERIALS AND METHODS—**Biopsy proven fibroadenomas (n=26) initially identified as suspicious on breast MRI were retrospectively evaluated. Histopathological assessments of lesion cellularity and stromal type were compared with ADC measures on diffusion-weighted MRI.

**RESULTS—**Presence of epithelial hyperplasia (increased cellularity) and dense collagenous stroma were both significantly associated with lower lesion ADC values (p=0.02 and 0.004, respectively.

**CONCLUSION—**Variations in epithelial cellularity and stromal type influence breast lesion ADC values and may explain the wide range of ADC measures observed in benign fibroadenomas.

### Keywords

Fibroadenomas; diffusion weighted imaging (DWI); apparent diffusion coefficient (ADC); cellularity; stroma

## 1. Introduction

As use of dynamic contrast enhanced (DCE) breast MRI increases due to its high sensitivity for breast cancer detection (1, 2), finding ways to decrease its false-positive rate becomes more pertinent to avoid unnecessary biopsies. Unfortunately, many benign pathologies presenting as suspicious enhancement cannot be discriminated from malignancy on the basis of morphologic and enhancement features alone. Therefore, the use of supplemental imaging information beyond standard DCE characteristics is actively being evaluated to reduce unnecessary patient morbidity and anxiety caused by avoidable breast biopsy.

Perhaps the most promising supplemental MRI technique is diffusion weighted imaging (DWI), which is a short, non-contrast sequence that measures the ability of water molecules to freely diffuse within tissue. Water diffusivity can be calculated through generation of apparent diffusion coefficients (ADCs), which are hypothesized to indirectly measure biological properties that could affect water diffusion including cellularity and stromal characteristics (3). In highly cellular or fibrotic lesions, water diffusion is thought to be more restricted. Breast cancers generally have higher cellularity than normal breast tissue or benign pathologies and therefore exhibit restricted water diffusion, with lower ADC values than reference normal breast parenchyma and benign breast lesions (4–6). The complementary information provided by DWI has the potential to further increase specificity of conventional breast MRI protocols by differentiating benign from malignant lesions based on their higher ADC values (7).

Fibroadenomas are benign solid tumors containing glandular and fibrous tissue and originate from intralobular stroma, with peak incidence between the ages of 15 and 35 years (8). Fibroadenomas may represent as high as 17% of all lesions and 29% of all masses presenting on DCE-MRI as false-positives (9). The majority of fibroadenomas can be confidently differentiated from malignancy with conventional imaging (mammography

and/or ultrasound), and biopsy is avoided when they exhibit typical benign morphology, such as round or oval shape, circumscribed margins and dark nonenhancing internal septations. Microscopically, fibroadenomas demonstrate biphasic growth with ductal and stromal proliferation. Epithelium within a fibroadenoma is hormonally responsive and may increase in size, infarct, or become inflamed (10), which may result in MRI features that overlap with those of malignancy. High signal on T2-weighted imaging has also been reported to be a useful feature for discriminating fibroadenomas from malignant masses. However, this feature is not pathognomonic for benignity (11), with some malignancies (e.g. mucinous subtype) also exhibiting high T2-weighted signal intensity. Moreover, progressive sclerosis and stromal hyalinization of fibroadenomas after menopause can reduce their signal intensity on T2-weighted images (12). Therefore, fibroadenomas continue to account for many unnecessary biopsies prompted by DCE-MRI.

Prior DWI studies have shown that the majority of fibroadenomas presenting as false-positive lesions on conventional breast MRI can be identified as benign based on high ADC values. However, some fibroadenomas exhibit lower ADC values in the indeterminate to malignant range, which limits DWI's potential to improve the positive predictive value of MRI (9). In this study, we sought to investigate the underlying histopathologic characteristics that influence ADC values of fibroadenomas presenting as false-positive lesions on conventional breast MRI.

## 2. Material and Methods

We have previously published our results investigating the clinical utility of breast DWI in differentiating high-risk subtypes from benign breast lesions (9). For this study, we further examined a subset of the lesions identified in that prior study, as described below.

### 2.1. Subjects and Lesions

This retrospective study was Health Insurance Portability and Accountability Act compliant and was approved by our local Institutional Review Board, which waived requirements for informed consent. As previously described (9), a retrospective review of our MRI database was performed to identify all consecutive suspicious breast lesions detected on breast MRI (BI-RADS category 4 or 5) from October of 2005 to December of 2008 that were subsequently sampled at core needle or surgical biopsy. In the prior study, 30/175 (17%) of false positive breast MRI lesions with DWI were fibroadenomas without atypia, which comprised the cohort for this current study.

Of the 30 fibroadenomas previously identified in 27 women, one lesion in one woman was excluded because pathology slides were unavailable at the time of the current study and three MRI lesions in another woman were excluded due to inability to retrospectively perform direct imaging-pathology correlation because the patient had multiple masses excised without prior core needle biopsy. Thus, the final cohort for this study included 26 fibroadenomas identified in 25 women. Figure 1 illustrates the patient selection process for the study.

### 2.2. MRI Protocol

MR acquisition and analysis procedures were described previously (9). Briefly, imaging was performed on a 1.5 tesla (T) scanner (LX; GE Healthcare, Waukesha, WI) using a dedicated 8-channel bilateral breast coil. All imaging was bilateral, acquired in axial orientation and included the following imaging sequences: T2-weighted fast spin echo sequence, T1-weighted non-fat suppressed sequence, T1-weighted DCE-MRI sequence (one pre-contrast and 3 to 5 post-contrast scans following injection of 0.1 mmol/kg body weight gadopentetate dimeglumine) and a DWI sequence. DCE was performed using a fat-suppressed T1-weighted three dimensional fast spoiled gradient-recalled echo sequence with parallel imaging (Volume Imaging for BReast Assessment, or VIBRANT) with repetition time msec/echo time (msec) = 6.2/3, flip angle =10°, field of view = 32–38 cm, section thickness = 1.6–2.2 mm. DWI was performed using an echo-planar imaging sequence with parallel imaging (Array Spatial Sensitivity Encoding Technique, or ASSET) and fat suppression (SPECtral Inversion at Lipids, or SPECIAL) with reduction factor = two; 7000/71.5; number of signals acquired = three, matrix = 192 × 192; field of view = 36 cm, section thickness = 5 mm and gap = 0. Diffusion gradients were applied in six directions using sensitization values (b) = 0 and 600 sec/mm$^2$ with the total imaging time of 2 minutes and 40 seconds.

### 2.3. Analysis of MR images

As previously described (9), DCE-MRI scans were prospectively interpreted by one of four fellowship-trained radiologists specializing in breast imaging, with radiologists blinded to lesion outcomes at the time of interpretation. Morphologic and enhancement kinetic features of included lesions were described following American College of Radiology (ACR) BI-RADS guidelines(13). Lesion characteristics including size and location, as well as the BI-RADS assessment and recommendation were recorded at the time of interpretation. Two research scientists, trained in quantitative analysis of breast MRI and blinded to the histopathologic diagnosis of each lesion, retrospectively analyzed the DW images. DCE images and clinical interpretation reports were used to identify the lesions on DWI. ADC maps were generated using in-house software and ADC values were measured for lesions and contralateral normal fibroglandular tissue, as previously described (9). Briefly, regions of interest (ROI) were defined separately for lesion and contralateral normal fibroglandular tissue on DWI and propagated to the ADC maps. The mean ADC of the voxels in each ROI was calculated to determine lesion and normal tissue ADC values.

Finally, the signal intensity on T2-weighted imaging for each individual fibroadenoma was retrospectively assessed qualitatively using ipsilateral axillary lymph nodes as an internal control. Fibroadenomas visually demonstrating T2-weighted signal intensity equal to or higher than that of axillary lymph nodes were categorized as hyperintense, while those lower than that of axillary lymph nodes were categorized as hypointense.

### 2.4. Detailed Histopathologic Analysis

Core needle biopsy samples for 24 fibroadenomas and excisional biopsy specimens for two fibroadenomas were reviewed by a pathologist, blinded to the lesion DWI characteristics. Detailed histopathologic analyses were performed on the hematoxylin and eosin slides,

assessing tissue cellularity (characterized by presence of epithelial hyperplasia, stromal cellularity, and immune cell infiltration) and stromal type defined as below:

1. Epithelial hyperplasia, which was categorized as present (Fig. 2B) or absent (Fig. 2A) depending on whether usual ductal hyperplasia (without atypia) was observed in epithelial ducts contained within the fibroadenomas, according to the criteria of Dupont and Page (14) and Page and Rogers (15).
2. Stromal cellularity, which was categorized as low (Fig. 2E) or high (Fig. 2D) based on a qualitative assessment of the number of fibroblast nuclei in a 10-times power (10X) field. The most cellular area of the pathology slide was assessed. Low stromal cellularity was defined as being approximately twice the cellularity of that of normal perilobular stroma, with no or scattered stromal nuclei appearing to touch. High stromal cellularity was defined as having more confluent stromal cells with many stromal cell nuclei appearing to touch.
3. Immune cell infiltration, which was categorized as present (Fig. 2F) or absent at 10X field, was defined as absent if very low or baseline numbers of inflammatory cells (lymphocytes, histiocytes, mast cells, plasma cells, neutrophils, or eosinophils) were observed and present if substantial numbers or collections of inflammatory cells were identified.
4. Stromal type, which was categorized as dense (collagenous/sclerotic) stroma (Fig. 2C, and 2A) or sparse (myxoid/loose) stroma (Fig. 2F) based on qualitative assessment of collagen deposition density.

### 2.5. Statistical Analysis

ADC values were compared for fibroadenomas versus normal fibroglandular tissue in each patient by using the Wilcoxon signed-rank test. Mean ADCs were then compared between groups based on epithelial hyperplasia (present vs. absent), stromal cellularity (low vs. high), immune cell infiltration (present vs. absent) and lesion stromal type (dense vs. sparse), using Wilcoxon Rank-Sum test. Correlations between histopathologic features were evaluated by Fisher's exact test. Fibroadenomas also were classified as DWI positive or negative based on a previously determined ADC threshold of $1.81\times10^{-3}$ $mm^2/s$ (16): those with ADC values lower than the predetermined threshold were classified as DWI false-positives, those with ADC greater than or equal to the threshold were classified as DWI true-negatives. Differences in histopathologic characteristics between DWI false-positive and true-negative lesions were assessed by Fisher's exact test. Exploratory multivariable logistic regression modeling was performed to identify histopathologic features independently associated with DWI positive or negative classification. A p-value $<0.05$ was considered statistically significant. Analyses were conducted using JMP software, version 9.0.2 (SAS Institute, Inc., Cary, NC).

# 3. Results

## 3.1 Subjects and lesions

Subjects ranged in age from 35 to 66 years (median age 46.5 years). The clinical indications for the MR imaging examinations were to evaluate extent of disease in patients with a new diagnosis of breast cancer in 13/25 (52%) subjects, high-risk screening in 10 (40%), evaluation for occult primary in one (4%) and problem solving in one (4%).

Of the 26 included fibroadenomas, two presented as non-mass enhancement (NME), 23 as masses and one as a focus. All 26 fibroadenomas were classified as suspicious (BI-RADS category 4). Maximum MRI lesion size for fibroadenomas (longest single dimension) ranged from 0.2 to 5.4 cm (median, 0.9 cm). Lesion characteristics are reported in Table 1.

Histologically, the majority of fibroadenomas demonstrated no epithelial hyperplasia (18/26 [69%]) or immune cell infiltration (17/26 [65%]) and low (n=21) or minimal (n=1) stromal cellularity (22/26 [85%]). The stromal type was dense in 14/26 (54%) of fibroadenomas. Among the 22 fibroadenomas exhibiting low stromal cellularity, 13 had dense stroma, eight had immune cell infiltration, and four had epithelial hyperplasia.

## 3.2. Lesion DWI and T2-weighted Imaging Characteristics

The mean ADC of the fibroadenomas was $1.98 \pm 0.42 \times 10^{-3}$ $mm^2/s$, which was not significantly different from normal fibroglandular tissue ($2.10 \pm 0.42 \times 10^{-3}$ $mm^2/s$, $p>0.05$). Nine (35%) of the fibroadenomas demonstrated ADC values below the predetermined ADC threshold ($1.81 \times 10^{-3}$ $mm^2/s$) and were thus deemed DWI false-positives. On T2-weighted imaging, 16 fibroadenomas were hyperintense while the remaining 10 were hypointense, relative to axillary lymph nodes. Of the fibroadenomas that were hyper-intense on T2 weighted images, 10/16 demonstrated either non-circumscribed margins or an irregular shape. Of the 16 fibroadenomas that were T2 hyperintense, 12 also demonstrated ADC above threshold. Of the 10 fibroadenomas that were T2 hypointense, five had ADC above threshold.

## 3.3. Correlation of Imaging Features of Fibroadenomas with Histopathology

Fibroadenomas with epithelial hyperplasia (n=8) demonstrated significantly lower mean ADC ($1.69 \pm 0.33 \times 10^{-3}$ $mm^2/sec$, Fig. 3, and 4) than fibroadenomas without epithelial hyperplasia (n= 18, ADC=$2.11 \pm 0.40 \times 10^{-3}$ $mm^2/sec$ and p=0.02, Fig. 7A). Additionally fibroadenomas with dense stroma (n=14) demonstrated significantly lower mean ADC ($1.76 \pm 0.42 \times 10^{-3}$ $mm^2/sec$, Fig. 3) than fibroadenomas with sparse stroma (n= 12, ADC=$2.25 \pm 0.23 \times 10^{-3}$ $mm^2/sec$ and p=0.004, Fig. 5, 6A and 6B). No significant correlation was found between mean ADC values and stromal cellularity or immune cell infiltration ($p>0.05$). Mean ADC values of fibroadenomas based on histopathologic characteristics are summarized in Table 2.

Presence of epithelial hyperplasia and dense stroma were not significantly correlated (p=0.68), and neither histopathologic feature was correlated with presence of immune cell

infiltration (p=0.67, p=0.22, respectively). Fibroadenomas with high stromal cellularity were more likely to have concurrent epithelial hyperplasia (p=0.005).

Of the 26 fibroadenomas presenting as suspicious enhancement on DCE-MRI, nine (35%) remained false-positive lesions on DWI based on an ADC threshold. Characteristics of DWI false-positive and true-negative fibroadenomas are summarized in Table 3. DWI false-positive fibroadenomas more often had dense stroma compared to the DWI true-negatives (9/9 vs. 5/17, p=0.0007). DWI false-positive lesions also tended to more often demonstrate epithelial hyperplasia compared to true-negatives (5/9 vs. 3/14, p=0.07). Differences in stromal cellularity and presence of immune cell infiltration between the two groups were not significant by univariate analyses (p>0.05). Multivariable logistic regression modeling identified presence of epithelial hyperplasia (p=0.009), immune cell infiltration (p=0.046), and dense stroma (p<0.0001) to be independently predictive of DWI false-positive classification.

## 4. Discussion

Fibroadenomas remain one of the most common lesions presenting as a false-positive finding on DCE-MRI (9). Although certain imaging characteristics, such as strong homogeneous signal on T2-weighted sequences and non-enhancing dark septations, are reported as characteristic of fibroadenomas, these findings are not present in many fibroadenomas and are not sufficiently specific to exclude malignancy as isolated features (17, 18). DWI has shown potential for differentiating benign and malignant lesions through the use of an ADC threshold (7). Integration of DWI into clinical assessment has been suggested to improve specificity and diagnostic accuracy of breast MRI (16, 19–21). Fibroadenomas commonly demonstrate high ADC values in the non-malignant range. However, for unclear reasons, many fibroadenomas exhibit low ADC within the malignant range (9).

In this study, we performed detailed histopathologic analysis of fibroadenomas presenting as false-positive DCE MRI findings to further understand the biological properties of fibroadenomas measured by DWI. We found ADC values on DWI to be significantly influenced by both epithelial hyperplasia and stromal type. We further observed that implementing a previously defined diagnostic ADC threshold, 17/26 fibroadenomas were correctly classified as benign based on high ADC (true-negatives). DWI false-positive lesions (those with ADC values below the threshold) more often exhibited epithelial hyperplasia and dense stroma than the true-negatives. Presence of immune cell infiltration was also incrementally associated with DWI false-positives in multivariable analysis. The lack of association between stromal cellularity and ADC may be explained by the fact that the majority of fibroadenomas in our cohort had low stromal cellularity, with only four exhibiting high stromal cellularity.

Fibroadenomas have been presumed to have higher ADC values than malignancies due to predominance of stromal myxoid changes resulting in sparse stroma and consequently higher water mobility (6), while predominance of the fibrous stromal component has been proposed as the reason some fibroadenomas exhibit low ADCs in the malignant range (5).

Our results agree with these hypotheses, as we found that fibroadenomas with sparse stroma exhibited higher ADC values. Furthermore, we found that fibroadenomas with epithelial hyperplasia exhibited significantly lower ADC values, which adds to the body of evidence linking higher cellularity of breast tumors with lower ADC values when compared to normal breast parenchyma and benign breast lesions (7, 22). Presence of immune cell infiltration in cases of mastitis, abscess or inflammatory carcinoma of the breast are reportedly associated with low ADC values (23, 24). While we did not observe a direct correlation with ADC, likely due to a lesser degree of immune cell infiltration in benign lesions (25), presence of immune cell infiltration was associated with lower ADC (DWI false-positives) in multivariable analysis.

Our study has several limitations. Lesion ADC was calculated from a single representative slice on DWI, and histopathologic analysis was performed on core needle biopsy samples rather than excisional biopsy specimens for most cases, both of which may incorporate sampling error and limit accuracy for lesion assessment. Furthermore, 66% (17/26) of the lesions measured less than 1 cm in maximum dimension and partial volume averaging may limit accuracy of ADC measures due to the relatively low spatial resolution of the DWI technique. Our study used a conventional ADC calculation approach based on monoexponential signal decay model, which includes both perfusion and diffusion effects. Advanced DWI modeling techniques to separate influences of perfusion, cellularity, and tissue complexity on diffusion measures may increase ability to differentiate lesions based on underlying biological features (3, 26–29). Finally, we only evaluated fibroadenomas presenting as false-positives on DCE MRI; therefore, the pathologic features found to be linked to ADC values in this study may not apply to clearly benign fibroadenomas identified on DCE MRI.

## 5. Conclusions

In summary, our findings demonstrate a clear association of ADC values obtained from breast DWI with specific biologic features of breast lesions. Among fibroadenomas presenting as suspicious enhancement on DCE-MRI, we found ADC values reflect variations in both cellularity and stromal composition. Combined with other imaging features, DWI may be helpful in improving radiology-pathology concordance of biopsied lesions and guiding personalized therapies.

## Acknowledgments

Supported by NIH grants R01-CA151326 and R01-CA164371.

Some of the data from this paper was presented as an oral presentation at the United States and Canadian Academy of Pathology on March 1-7 2014, San Diego, CA and parts of the data were published in Radiology. 2012 Dec; 265(3): 696-706. Epub 2012 Oct 2. Supported by: NIH grants R01-CA151326 and R01-CA164371.

## References

1. Lehman CD, Isaacs C, Schnall MD, Pisano ED, Ascher SM, Weatherall PT, et al. Cancer yield of mammography, MR, and US in high-risk women: prospective multi-institution breast cancer screening study. Radiology. 2007; 244(2):381–8. DOI: 10.1148/radiol.2442060461 [PubMed: 17641362]

2. Kriege M, Brekelmans CT, Boetes C, Besnard PE, Zonderland HM, Obdeijn IM, et al. Efficacy of MRI and mammography for breast-cancer screening in women with a familial or genetic predisposition. The New England journal of medicine. 2004; 351(5):427–37. DOI: 10.1056/NEJMoa031759 [PubMed: 15282350]

3. Le Bihan D, Breton E, Lallemand D, Aubin ML, Vignaud J, Laval-Jeantet M. Separation of diffusion and perfusion in intravoxel incoherent motion MR imaging. Radiology. 1988; 168(2):497–505. [PubMed: 3393671]

4. Guo Y, Cai YQ, Cai ZL, Gao YG, An NY, Ma L, et al. Differentiation of clinically benign and malignant breast lesions using diffusion-weighted imaging. J Magn Reson Imaging. 2002; 16(2):172–8. [PubMed: 12203765]

5. Kinoshita T, Yashiro N, Ihara N, Funatu H, Fukuma E, Narita M. Diffusion-weighted half-Fourier single-shot turbo spin echo imaging in breast tumors: differentiation of invasive ductal carcinoma from fibroadenoma. Journal of computer assisted tomography. 2002; 26(6):1042–6. [PubMed: 12488758]

6. Sinha S, Lucas-Quesada FA, Sinha U, DeBruhl N, Bassett LW. In vivo diffusion-weighted MRI of the breast: potential for lesion characterization. J Magn Reson Imaging. 2002; 15(6):693–704. [PubMed: 12112520]

7. Chen X, Li WL, Zhang YL, Wu Q, Guo YM, Bai ZL. Meta-analysis of quantitative diffusion-weighted MR imaging in the differential diagnosis of breast lesions. BMC cancer. 2010; 10:693.doi: 10.1186/1471-2407-10-693 [PubMed: 21189150]

8. Carty NJ, Carter C, Rubin C, Ravichandran D, Royle GT, Taylor I. Management of fibroadenoma of the breast. Annals of the Royal College of Surgeons of England. 1995; 77(2):127–30. [PubMed: 7793802]

9. Parsian S, Rahbar H, Allison KH, Demartini WB, Olson ML, Lehman CD, et al. Nonmalignant breast lesions: ADCs of benign and high-risk subtypes assessed as false-positive at dynamic enhanced MR imaging. Radiology. 2012; 265(3):696–706. DOI: 10.1148/radiol.12112672 [PubMed: 23033500]

10. Tse, G. Fine needle aspiration cytology of the breast: atlas of cyto-histologic correlates. New York: Springer; 2013.

11. Westra C, Dialani V, Mehta TS, Eisenberg RL. Using T2-weighted sequences to more accurately characterize breast masses seen on MRI. AJR Am J Roentgenol. 2014; 202(3):W183–90. DOI: 10.2214/AJR.13.11266 [PubMed: 24555613]

12. Kuhl CK, Klaschik S, Mielcarek P, Gieseke J, Wardelmann E, Schild HH. Do T2-weighted pulse sequences help with the differential diagnosis of enhancing lesions in dynamic breast MRI? J Magn Reson Imaging. 1999; 9(2):187–96. [PubMed: 10077012]

13. Morris, EA.; CC; Lee, CH., et al. ACR BI-RADS® Atlas, Breast Imaging Reporting and Data System. Reston, VA: American College of Radiology; 2013. ACR BI-RADS® Magnetic Resonance Imaging.

14. Dupont WD, Page DL. Risk factors for breast cancer in women with proliferative breast disease. The New England journal of medicine. 1985; 312(3):146–51. DOI: 10.1056/NEJM198501173120303 [PubMed: 3965932]

15. Page DL, Rogers LW. Combined histologic and cytologic criteria for the diagnosis of mammary atypical ductal hyperplasia. Hum Pathol. 1992; 23(10):1095–7. [PubMed: 1328030]

16. Partridge SC, DeMartini WB, Kurland BF, Eby PR, White SW, Lehman CD. Quantitative diffusion-weighted imaging as an adjunct to conventional breast MRI for improved positive predictive value. AJR Am J Roentgenol. 2009; 193(6):1716–22. DOI: 10.2214/AJR.08.2139 [PubMed: 19933670]

17. Yuen S, Uematsu T, Kasami M, Tanaka K, Kimura K, Sanuki J, et al. Breast carcinomas with strong high-signal intensity on T2-weighted MR images: pathological characteristics and differential diagnosis. J Magn Reson Imaging. 2007; 25(3):502–10. DOI: 10.1002/jmri.20845 [PubMed: 17326093]

18. Santamaria G, Velasco M, Bargallo X, Caparros X, Farrus B, Luis Fernandez P. Radiologic and pathologic findings in breast tumors with high signal intensity on T2-weighted MR images. Radiographics. 2010; 30(2):533–48. DOI: 10.1148/rg.302095044 [PubMed: 20228333]

19. Ei Khouli RH, Jacobs MA, Mezban SD, Huang P, Kamel IR, Macura KJ, et al. Diffusion-weighted imaging improves the diagnostic accuracy of conventional 3.0-T breast MR imaging. Radiology. 2010; 256(1):64–73. DOI: 10.1148/radiol.10091367 [PubMed: 20574085]

20. Pinker K, Bickel H, Helbich TH, Gruber S, Dubsky P, Pluschnig U, et al. Combined contrast-enhanced magnetic resonance and diffusion-weighted imaging reading adapted to the “Breast Imaging Reporting and Data System” for multiparametric 3-T imaging of breast lesions. Eur Radiol. 2013; 23(7):1791–802. DOI: 10.1007/s00330-013-2771-8 [PubMed: 23504036]

21. Baltzer A, Dietzel M, Kaiser CG, Baltzer PA. Combined reading of Contrast Enhanced and Diffusion Weighted Magnetic Resonance Imaging by using a simple sum score. Eur Radiol. 2016; 26(3):884–91. DOI: 10.1007/s00330-015-3886-x [PubMed: 26115653]

22. Dorrius MD, Dijkstra H, Oudkerk M, Sijens PE. Effect of b value and pre-admission of contrast on diagnostic accuracy of 1.5-T breast DWI: a systematic review and meta-analysis. Eur Radiol. 2014; 24(11):2835–47. DOI: 10.1007/s00330-014-3338-z [PubMed: 25103535]

23. Woodhams R, Ramadan S, Stanwell P, Sakamoto S, Hata H, Ozaki M, et al. Diffusion-weighted imaging of the breast: principles and clinical applications. Radiographics. 2011; 31(4):1059–84. DOI: 10.1148/rg.314105160 [PubMed: 21768239]

24. de Bazelaire C, Groheux D, Chapellier M, Sabatier F, Scemama A, Pluvinage A, et al. Breast inflammation: indications for MRI and PET-CT. Diagn Interv Imaging. 2012; 93(2):104–15. DOI: 10.1016/j.diii.2011.12.004 [PubMed: 22305594]

25. Ben-Hur H, Cohen O, Schneider D, Gurevich P, Halperin R, Bala U, et al. The role of lymphocytes and macrophages in human breast tumorigenesis: an immunohistochemical and morphometric study. Anticancer Res. 2002; 22(2B):1231–8. [PubMed: 12168931]

26. Iima M, Yano K, Kataoka M, Umehana M, Murata K, Kanao S, et al. Quantitative Non-Gaussian Diffusion and Intravoxel Incoherent Motion Magnetic Resonance Imaging: Differentiation of Malignant and Benign Breast Lesions. Investigative radiology. 2014; doi: 10.1097/RLI.0000000000000094

27. Jensen JH, Helpern JA. MRI quantification of non-Gaussian water diffusion by kurtosis analysis. NMR in biomedicine. 2010; 23(7):698–710. DOI: 10.1002/nbm.1518 [PubMed: 20632416]

28. Bokacheva L, Kaplan JB, Giri DD, Patil S, Gnanasigamani M, Nyman CG, et al. Intravoxel incoherent motion diffusion-weighted MRI at 3.0 T differentiates malignant breast lesions from benign lesions and breast parenchyma. J Magn Reson Imaging. 2014; 40(4):813–23. DOI: 10.1002/jmri.24462 [PubMed: 24273096]

29. Liu C, Liang C, Liu Z, Zhang S, Huang B. Intravoxel incoherent motion (IVIM) in evaluation of breast lesions: comparison with conventional DWI. Eur J Radiol. 2013; 82(12):e782–9. DOI: 10.1016/j.ejrad.2013.08.006 [PubMed: 24034833]

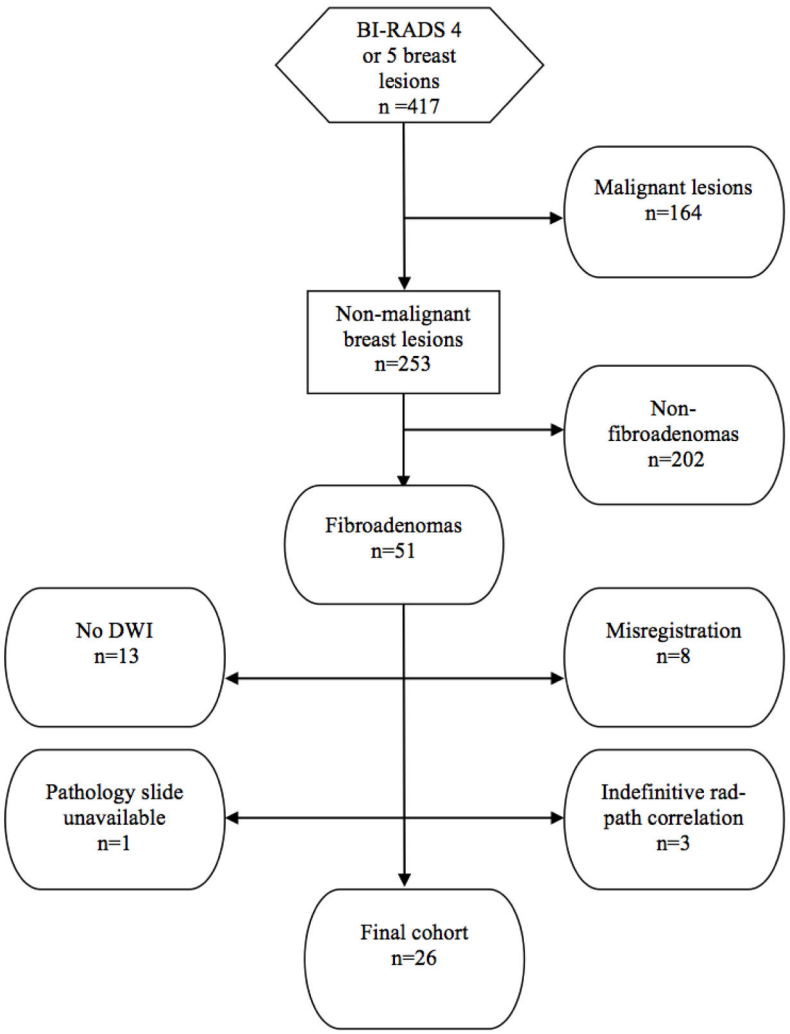


**Fig. 1.**

Diagram demonstrating patient selection for the study. These patients were the subgroup of women with fibroadenomas, identified from a larger cohort of women with false positive lesions described in detail in a prior study (9).

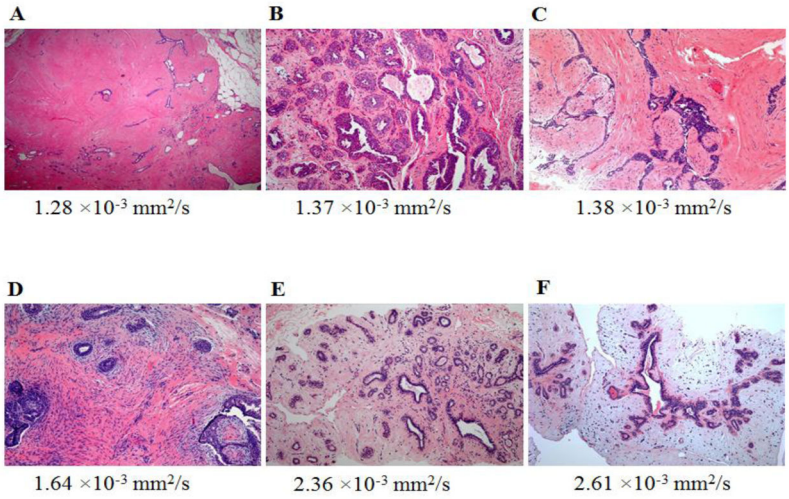


**Fig. 2.**

Hematoxylin-eosin stained slides of representative fibroadenomas with original magnification ×100 and their corresponding ADC values:

**A**, 65-year-old woman with personal history of right-breast invasive ductal carcinoma, status post lumpectomy with an MRI-detected fibroadenoma in the left breast exhibiting no epithelial hyperplasia, low stromal cellularity, no immune cell infiltration and dense stroma.

**B**, 49-year-old woman with personal history of right-breast invasive ductal carcinoma, status post lumpectomy, with an MRI-detected fibroadenoma in the left breast exhibiting epithelial hyperplasia, high stromal cellularity, no immune cell infiltration and dense stroma.

**C**, 48-year-old woman with personal history of left-breast lobular carcinoma in situ, status post lumpectomy, with an MRI-detected fibroadenoma in the right breast exhibiting epithelial hyperplasia, low stromal cellularity, no immune cell infiltration and dense stroma.

**D**, 35-year-old woman with personal history of left-breast ductal carcinoma in situ, status post lumpectomy, with an MRI-detected fibroadenoma in the right breast exhibiting epithelial hyperplasia, high stromal cellularity, no immune cell infiltration and dense stroma.

**E**, 35-year-old woman undergoing neoadjuvant chemotherapy for right breast inflammatory ductal carcinoma, with an MRI-detected fibroadenoma in the left breast exhibiting no epithelial hyperplasia, low stromal cellularity, no immune cell infiltration and sparse stroma.

**F**, 40-year-old high-risk woman with an MRI-detected fibroadenoma in the left breast exhibiting epithelial hyperplasia, low stromal cellularity, immune cell infiltration and sparse stroma.

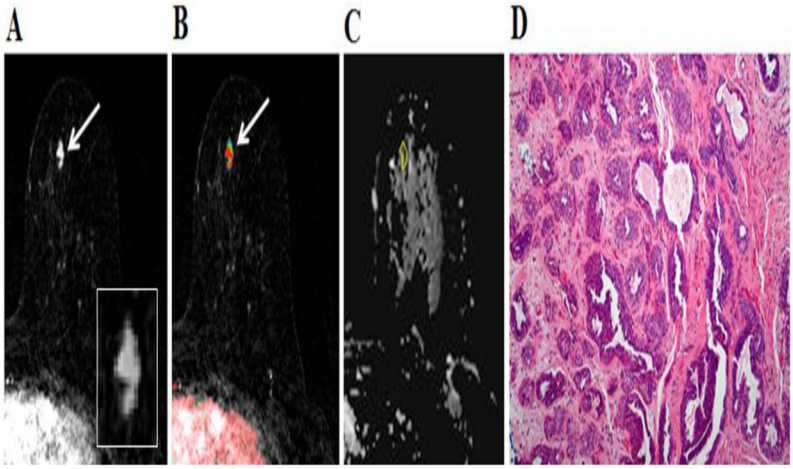


**Fig. 3.**

49-year-old woman with personal history of right-breast invasive ductal carcinoma, status post lumpectomy. The patient underwent breast MR imaging for high-risk screening. **A,** Axial dynamic contrast-enhanced initial post-contrast subtraction MR image with magnified inset shows 11-mm lobular homogeneously enhancing mass (arrow) at 11 o'clock of the left breast, 32-mm from the nipple. The lesion has a smooth margin and is at an anterior depth. This lesion was classified as BI-RADS category 4. **B,** Axial dynamic contrast-enhanced MR image shows the lesion (arrow) has mixed kinetics overall: rapid initial uptake with delayed washout enhancement (red). **C**, ADC map shows the lesion exhibits low ADC (mean, = 1.37 $\times 10^{-3}$ $mm^2/s$), measured within the corresponding region-of-interest (yellow contour). The lesion was classified as fibroadenoma on the basis of **D,** US-guided core biopsy. Hematoxylin-eosin stain with original magnification, ×100 demonstrates epithelial hyperplasia, high stromal cellularity, no immune cell infiltration and dense stroma.

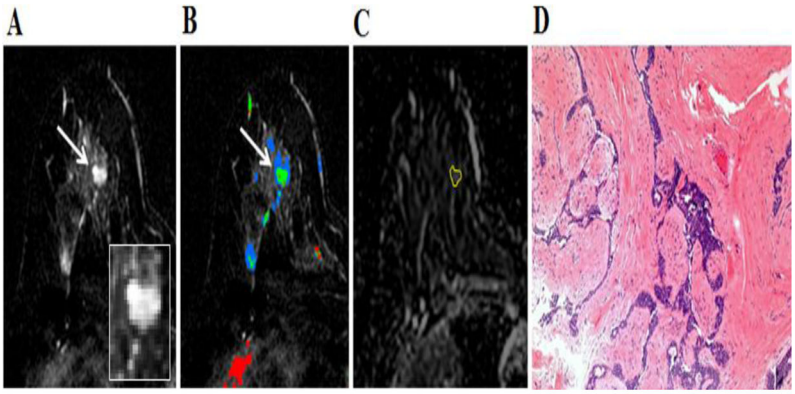


**Fig. 4.**

48-year-old woman with personal history of left-breast lobular carcinoma in situ status post lumpectomy. The patient underwent breast MR imaging for evaluation of left nipple thickening. **A,** Axial dynamic contrast-enhanced initial post-contrast subtraction MR image with magnified inset shows a new 9-mm homogeneously enhancing mass with dark internal septations (arrow) at 12 o'clock of the right breast, 46-mm from the nipple. The lesion has smooth margin and is at middle depth. This lesion was classified as BI-RADS category 4. **B,** Axial dynamic contrast-enhanced MR image shows the lesion (arrow) has predominantly persistent enhancement (green). **C,** ADC map shows the lesion exhibits low ADC (mean, = $1.38 \times 10^{-3}$ $mm^2/s$), measured within the corresponding region-of-interest (yellow contour). The lesion was classified as fibroadenoma on the basis of ultrasound-guided core biopsy. **D,** Hematoxylin-eosin stain with original magnification, ×100 demonstrates epithelial hyperplasia, low stromal cellularity, no immune cell infiltration and dense stroma.

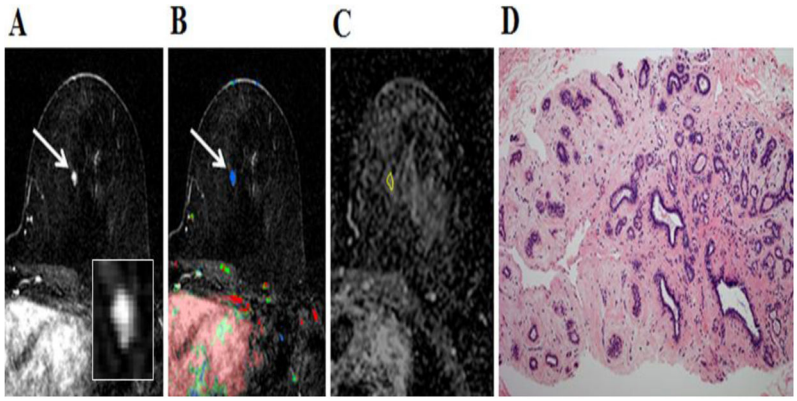


**Fig. 5.**

35-year-old woman with personal history of right breast inflammatory ductal carcinoma on neoadjuvant chemotherapy. The patient underwent breast MR imaging for high-risk screening. **A,** Axial dynamic contrast-enhanced initial post-contrast subtraction MR image with magnified inset shows a new 7-mm homogeneously enhancing mass (arrow) at 8 o'clock of the left breast, 56-mm from the nipple. The lesion has smooth margin and is at middle depth. This lesion was classified as BI-RADS category 4. **B,** Axial dynamic contrast-enhanced MR image shows the lesion (arrow) has mixed kinetics overall: medium initial uptake with predominantly delayed persistent enhancement (blue). **C,** ADC map shows the lesion exhibits high ADC (mean, = 2.36 $\times 10^{-3}$ $mm^2/s$), measured within the corresponding region-of-interest (yellow contour). The lesion was classified as fibroadenoma on the basis of ultrasound-guided core biopsy. **D,** Hematoxylin-eosin stain with original magnification, ×100 demonstrates epithelial hyperplasia, low stromal cellularity, no immune cell infiltration and loose stroma.

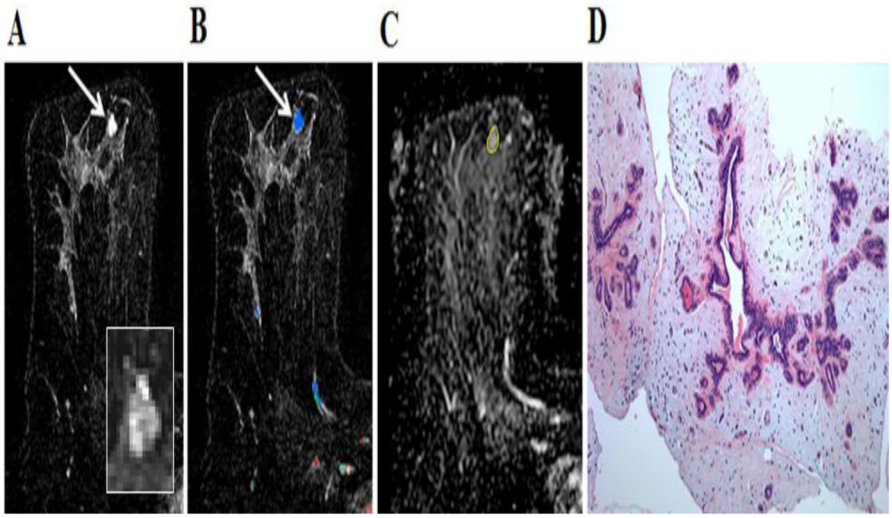


**Fig. 6.**

40-year-old woman who underwent breast MR imaging for high-risk screening. **A,** Axial dynamic contrast-enhanced initial post-contrast subtraction MR image with magnified inset shows a new 9-mm homogeneously enhancing oval mass (arrow) at 12 o'clock of the left breast, 49-mm from the nipple. The lesion has irregular margin and is at an anterior depth. This lesion was classified as BI-RADS category 4. **B,** Axial dynamic contrast-enhanced MR image shows the lesion (arrow) has mixed kinetics overall: medium initial uptake with predominantly delayed persistent enhancement (blue). **C,** ADC map shows the lesion exhibits high ADC (mean, = 2.61 $\times 10^{-3}$ $mm^2/s$), measured within the corresponding region-of-interest (yellow contour). The lesion was classified as fibroadenoma on the basis of ultrasound-guided core biopsy. **D,** Hematoxylin-eosin stain with original magnification, ×100 demonstrates epithelial hyperplasia, no stromal cellularity, no immune cell infiltration and sparse stroma.

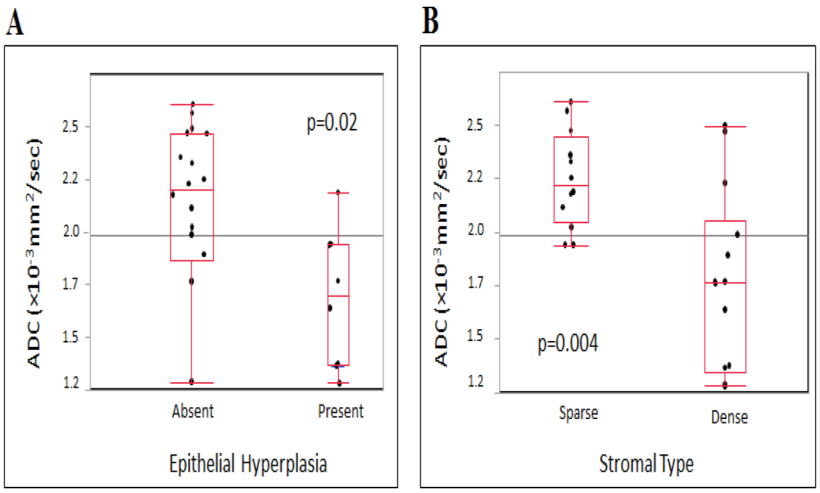


**Fig. 7.**

ADC values versus histologic features in fibroadenomas presenting as suspicious on DCE-MRI. Box plots represent medians and ranges of lesion ADCs. **A,** Fibroadenomas with epithelial hyperplasia (present) demonstrated significantly lower mean ADC (ADC=1.7 ±0.32 [standard deviation]×$10^{-3}$ $mm^2$/sec) than fibroadenomas without epithelial hyperplasia (absent; ADC=2.1 ±0.40×$10^{-3}$ $mm^2$/sec, p=0.02). **B,** Fibroadenomas with dense stroma demonstrated significantly lower mean ADC (ADC=1.7 ±0.42 [standard deviation] ×$10^{-3}$ $mm^2$/sec) than fibroadenomas with sparse stroma (ADC=2.2 ±0.23×$10^{-3}$ $mm^2$/sec, p=0.004).

**Table 1**

Lesion characteristics (n = 26).

| | n | (%) |
|---|---|---|
| BI-RADS Assessment | | |
| BI-RADS 4 | 26 | 100 % |
| Size (maximum diameter) | | |
| ≤ 0.5 cm | 1 | 4 % |
| 0.6 cm – 1 cm | 16 | 62 % |
| 1.1 cm – 2 cm | 5 | 19 % |
| > 2 cm | 4 | 15 % |
| Type | | |
| Focus | 1 | 4 % |
| Mass | 23 | 88 % |
| Shape: | | |
| Oval | 14 | |
| Round | 1 | |
| Irregular | 8 | |
| Margin: | | |
| Circumscribed | 9 | |
| Not circumscribed | 14 | |
| Internal Enhancement: | | |
| Homogeneous | 4 | |
| Heterogeneous | 19 | |
| Non-mass-like enhancement | 2 | 8 % |
| Distribution: | | |
| Focal | 2 | |
| Other | 0 | |
| Internal Enhancement: | | |
| Homogeneous | 0 | |
| Heterogeneous | 2 | |

Abbreviations: BI-RADS = Breast Imaging Reporting and Data System, ADC = apparent diffusion coefficient

## Table 2

Comparison of apparent diffusion coefficient values with histopathologic characteristics of fibroadenomas

| Histopathologic Parameter | Categories | n | Mean ADC± SD ($10^{-3}$ $mm^2/s$) | p-value |
|---|---|---|---|---|
| **Epithelial Hyperplasia** | Present | 8 | 1.69 ± 0.33 | 0.02 |
| | Absent | 18 | 2.11 ± 0.40 | |
| **Stromal Cellularity** | Low | 22 | 1.99 ± 0.45 | 0.59 |
| | High | 4 | 1.92 ± 0.22 | |
| **Immune Cell Infiltration** | Present | 9 | 2.03 ± 0.39 | 0.74 |
| | Absent | 17 | 1.96 ± 0.45 | |
| **Stromal Type** | Sparse | 12 | 2.25 ± 0.23 | 0.004 |
| | Dense | 14 | 1.76 ± 0.42 | |

Abbreviations: ADC= apparent diffusion coefficient, SD=standard deviation

**Table 3**

Comparison of histopathologic characteristics of fibroadenomas exhibiting ADC above or below a predetermined ADC malignancy threshold

| Histopathologic Parameter | Categories | n | ADC threshold ($1.81\times10^{-3}$ $mm^2/s$) (1) | | p-value |
|---|---|---|---|---|---|
| | | | N above (17 total) | N below (9 total) | |
| **Epithelial Hyperplasia** | Present | 8 | 3 | 5 | 0.07 |
| | Absent | 18 | 14 | 4 | |
| **Stromal Cellularity** | Low | 22 | 14 | 8 | 1.00 |
| | High | 4 | 3 | 1 | |
| **Immune Cell Infiltration** | Present | 9 | 6 | 3 | 1.0 |
| | Absent | 17 | 11 | 6 | |
| **Stromal Type** | Sparse | 12 | 12 | 0 | 0.0007 |
| | Dense | 14 | 5 | 9 | |

Abbreviations: ADC= apparent diffusion coefficient, SD=standard deviation